British Journal of Applied Science & Technology
7(1): 14-30, 2015, Article no.BJAST.2015.122
ISSN: 2231-0843

SCIENCEDOMAIN *international*
www.sciencedomain.org

Efficient Open Isobaric Expansion Based Thermal Cycles at Low Temperatures

Ramon Ferreiro Garcia[1*], Beatriz Ferreiro Sanz[1] and Cristina Ferreiro Sanz[1]

[1]Department of Industrial Engineering, ETSNM, Paseo de Ronda 51, 15011, University of A Coruna, Spain.

Authors' contributions

This work was carried out in collaboration between all authors. Author RFG designed the study, wrote the protocol, the first draft of the manuscript and managed literature searches. Authors BFS and CFS managed the analyses of the study and literature searches. All authors read and approved the final manuscript.

Article Information

DOI: 10.9734/BJAST/2015/13696
Editor(s):
(1) João Miguel Dias, Habilitation in Department of Physics, CESAM, University of Aveiro, Portugal.
(2) Harry E. Ruda, Centre for Advanced Nanotechnology, University of Toronto, Canada.
Reviewers:
(1) Roberto Capata, Department of Mechanical & Aerospace Engineering, University of Roma "Sapienza", Italy.
(2) Anonymous, China.
(3) Anonymous, Taiwan.
(4) Enhua Wang, State Key Laboratory of Automotive Safety and Energy, Tsinghua University, China.
Complete Peer review History: http://www.sciencedomain.org/review-history.php?iid=770&id=5&aid=7694

Original Research Article

Received 29th August 2014
Accepted 19th December 2014
Published 9th January 2015

ABSTRACT

The work aims to provide feasible structures for the open processes based thermal cycle as well as the regenerative open processes based thermal cycle characterised by rendering high thermal efficiency at low temperatures. Both cycles differ from the conventional Carnot-based thermal cycles (Carnot, Otto, Diesel, Rankine, Brayton, Stirling, Ericsson, and variants of these cycles) in that the conversion of heat to mechanical work is performed undergoing load reaction based path functions which means an isobaric expansion process at constant load in which thermal energy absorption and conversion to mechanical work are performed simultaneously along a single transformation of the cycle, contrary to what happens in conventional Carnot-based engines, in which mechanical work is delivered by means of a quasi-entropic expansion along a single transformation. Because of the mentioned differences these cycles do not obey the Carnot statement.
A performance analysis of the OPTC and the ROPTC operating with hydrogen, helium, and nitrogen was carried out and the results were compared with those for a Carnot cycle operating

**Corresponding author: E-mail: ferreiro@udc.es;*

under the same range of temperatures. High theoretical thermal efficiency was achieved for the ROPTC, surpassing the Carnot factor under favourable conditions. These results, obtained with a structurally simple and compact engine, pave the way for a new generation of power convertors.

Keywords: Carnot factor; isobaric expansion; open process; regeneration; thermal efficiency.

Nomenclature	Acronyms	
T Temperature (K)	*CF*	*Carnot factor*
p Pressure (bar)	*ORC*	*Organic Rankine cycle*
h Specific enthalpy (kJ/kg)	*NORC*	*Non-organic Rankine cycle*
s Specific entropy (kJ/kg-K)	*OPTC*	*Trilateral thermal cycle*
V Volume (m^3)	*ROPTC*	*Regenerative trilateral thermal cycle*
v Specific volume (m^3/kg)	*2p3w*	*Two-positions, three-way valve*
η_{NR} Non-regenerative OPTC thermal efficiency (%)	*WF*	*Working fluid*
η ROPTC thermal efficiency (%)	*ICE*	*Internal combustion engine*
C_R Conversion ratio (%)	*T_L*	*Cycle bottoming temperature*
q Specific heat energy (kJ/kg)	*T_H*	*Cycle top temperature*
Cp Specific heat at constant pressure (kJ/kg-K)		
Cv Specific heat at constant volume (kJ/kg-K)		
γ Adiabatic expansion coefficient (Cp/Cv)		
Pr Pressure ratio [p_2/p_1]		

1. INTRODUCTION

The limitations imposed by the Carnot statement to the thermal efficiency are especially relevant to all thermal cycles that operate at low temperatures, constraining its economic viability and applicability. Among the cycles that operate with residual heat including the low temperature power sources, are those known as bottoming ORCs (organic Rankine cycles). They constituted so far an interested energy conversion option, having shown acceptable thermodynamic performance for bottoming cycles [1,2]. The interest in organic WFs for residual heat applications with low temperature Rankine cycles is an old technique that has been proposed for different applications such as renewable energy and low temperature heat recovery [3-6]. Recent advances concerning low grade heat sources applied to ORCs include the works of Wang and colleagues [7], who compared several WFs for low-temperature ORCs, concluding that R123 is the best choice for the temperature range of 100 to 180ºC and R141b is the optimal working fluid when the temperature is higher than 180ºC. In the same way, Jianqin and colleagues [8] proposed using an open steam power cycle for internal combustion engine exhaust gas energy recovery, where the authors concluded that the recovery efficiency of exhaust gas heat is mainly limited by exhaust gas temperatures. However the thermal efficiency can be improved.

In the study carried out by Dongxiang and colleagues [9] it is proposed an ideal ORC to analyse the influence in working fluid properties on thermal efficiency. The optimal operating conditions and exergy destruction for various heat source temperatures were also evaluated by means of pinch point analysis and exergy analysis. The results showed that different WFs have little impact on the optimal operating condition of ORC and selection of working fluid reasonably based on heat source temperature will help to optimise ORC performance.

For intermediate temperature thermo-solar power plants, ORCs operating as bottoming cycles in combined power plants were proposed previously by [10], who analysed a combination of ORC fluids and cycle layouts that resulted in a global combined cycle efficiency slightly below 45.2%. This bottoming ORC has been studied in [11] with a carbon dioxide topping cycle, and in [12-14] for ORCs operating with micro turbine-based combined cycles.

All thermodynamic cycles including the proposed cycle in this work are subjected to the constraints imposed by the second law, that sets limits on the possible efficiency of the thermal cycles determining the direction of energy flow [15]. Despite these restrictions, residual or waste heat characterised by low-grade thermal energy (moderately low temperatures) can still be very useful on an industrial scale [16].

Given that biological mechanisms convert the biochemical energy of food into mechanical work under a very low temperature ratio, which violates Carnot's statement, it is fair to assume that if nature has developed such efficient cycles (engines) the development of more efficient artificial thermal cycles might also be possible. If muscles are seen as engines, speculation on the principles governing energy efficiency is an obvious natural corollary. It has appeared to many researchers that muscles achieve higher efficiency than the Carnot factor given as ($1-T_L/T_H$ with T_L/T_H as the ratio of the top to the bottom cycle temperatures) of a reversible Carnot engine. In animal muscles, energy conversion processes consist of biochemical transformations instead of thermodynamic transformations. Consequently, it may be possible to achieve higher efficiency in artificial engines than would be supposed from conventional Carnot engines by applying energy conversion cycles that differ from those of quadrilateral Carnot cycles. This respects the fact that Kelvin's results do not apply to every type of energy convertor, but only to heat engines, that is, engines which operate by converting heat from a reservoir at a given temperature and delivering expansion-based mechanical work and heat to a reservoir at lower temperature. Nevertheless, there is no reason why the Carnot factor should not apply to engines that deliver mechanical work while absorbing heat simultaneously undergoing a load reaction based path function (isobaric path function at constant reaction load). Indeed, the most universally available source of work, animal muscle, exhibits (based on simple observations like Clausius and Kelvin-Planck statements) a seemingly flagrant violation of the Carnot factor constraints.

According to the second law statements, the Carnot factor is not considered at all, as can be observed from the Kelvin Planck and Clausius statements, which are negative statements and therefore cannot be proved. Therefore, the second law, like the first, is based on experimental observations. As a consequence, if the process of a thermal cycle is irreversible, the thermal cycle must necessarily be irreversible. Conversely, if all processes of a cycle are reversible, the cycle is reversible. Nevertheless, experimental observations suggest that no process of a real thermal cycle is reversible.

All the conventional thermal cycles in use so far derive from the Carnot engine; that is, they are cycles in which ideally heat is absorbed at constant temperature (the top temperature) and work is delivered when the temperature decreases nearly to the bottom temperature. The power cycles that obey this model are classified into two main groups based on the nature of the working fluid (WF): Gas power cycles and vapour power cycles. The difference between the two groups is that in the first case the WF is gaseous and does not experience any phase change, whereas in the second there is a liquid–vapour phase change in the WF within the cycle. Fig. 1 depicts a simple classification of heat engines based on conventional Fig. 1(a) and non conventional thermal cycles Fig. 1(b). The non conventional thermal cycles depicted in Fig. 1(b) are not assumed as Carnot engines and may be also classified into two groups: Non regenerative and regenerative open processes based thermal cycles. While conventional thermal cycles satisfy the constraints imposed by the Carnot statement, thermal cycles not classified as Carnot cycles do not obey the Carnot statement while not violating the first and second principles of thermodynamics.

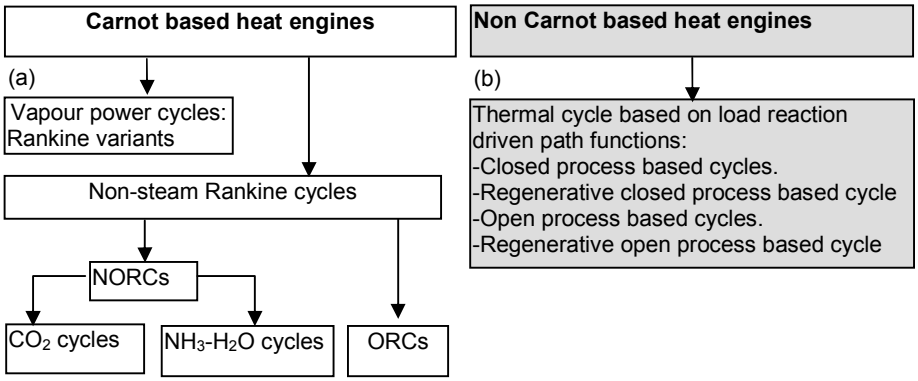

Fig. 1. Classification of the thermal engine cycles

Only Carnot engines based on quadrilateral thermal cycles have been considered so far open processes based cycles and an important question is therefore whether it is possible to implement thermal engines based on open processes that operate with cycles that yield higher efficiency than the Carnot engine. In what follows it will be shown that it is possible to implement thermal cycles technically capable of superseding the Carnot engines.

Thermal cycles that do not obey to the Carnot factor constraints have been recently described in [17,18,19], particularly characterised by its thermodynamic processes, which consists of closed and open process based transformations. However thermal cycles capable for superseding Carnot factor which undergoes open processes (this paper) have not been studied yet. The proposed gas cycle may be implemented as an open process based trilateral cycle. It is a thermal cycle which cannot be compared with a Carnot cycle since the proposed trilateral cycle absorbs energy and delivers work simultaneously along an open process based transformation, consisting of an isobaric path function at constant load, whereas the Carnot cycle absorbs energy and delivers work in two different and independent transformations. In the developed prototype, a thermal and a hydraulic cycle are coupled by means of two cylinders (thermal and hydraulic) and has the ability to convert thermal energy to hydraulic potential energy and, further, to electric power by means of hydraulic motor-generators or turbo-generators.

The work is organised in four main sections. Section 2 is devoted to the description of the concepts included in the proposed contribution, dealing with non-condensing mode thermal engines that do not obey the Carnot statement. In subsequent sub-sections, performance analysis is carried out for the open processes based thermal cycle (OPTC) and the regenerative open processes based thermal cycle (ROPTC). In Section 3, the results of the analysis of the cycle are applied to a case study dealing with the OPTC and ROPTC, followed by an analysis and discussion of the results. Section 4 concludes the paper.

2. THE OPTC: A THERMAL CYCLE INDEPENDENT OF THE CARNOT FACTOR

Since the only operating thermal engines known so far are those classified in Fig. 1 and mentioned in Section 1 which obeys the Carnot statement, this section introduces a class of thermal engines characterised by their ability to violate the Carnot statement without violating the second law. In order to show the behaviour of a generic OPTC to which the Carnot statement does not apply, the case of a single double-acting piston designed to develop work under a constant load-based path function (isobaric path function at constant load) along its active stroke is described.

2.1 Analysis of Heating Process Following an Isobaric Path Function under Closed and Open Processes Based Transformations

2.1.1 The closed processes based transformations

In order to show the basic relationship or the coupling effect between heat energy and mechanical work carried out under an isobaric path function, two cases dealing with closed and open processes respectively are analysed. The analysis of the closed system shown in Fig. 2 considers a thermal power source supplying heat to a cylinder piston operating with a WF (helium, nitrogen, or hydrogen). Since the gas is confined to the heater-cylinder control volume, which guarantees that no mass flow transfer exists, the heating or cooling process constitutes a closed system model. We are interested in determining the fraction of supplied heat that is converted into mechanical work along the transformation (2)–(3), defined as the conversion ratio (η_{23}).

Taking into account that losses due to isentropic efficiency in isobaric expansion-based transformations do not exist, let us assume that heat is added to a unit mass of WF following an isobaric path function from the state point (2) to the state point (3), as shown in Fig. 2, and suppose the resulting expansion causes the specific volume, temperature, enthalpy and entropy to change from state (2) to state (3). The first principle for a closed system where irreversibilities and potential and kinetic energy are neglected yields.

$$q_{23} - W_{23} = \Delta u_{23} = u_3 - u_2 \tag{1}$$

where the work W_{23} done by a unit mass of the WF is defined as

$$W_{23} = \int_{V2}^{V3} p \cdot dv = p_2(V_3 - V_2) = p_3(V_3 - V_2) = q_{23} - \Delta u_{23} \tag{2}$$

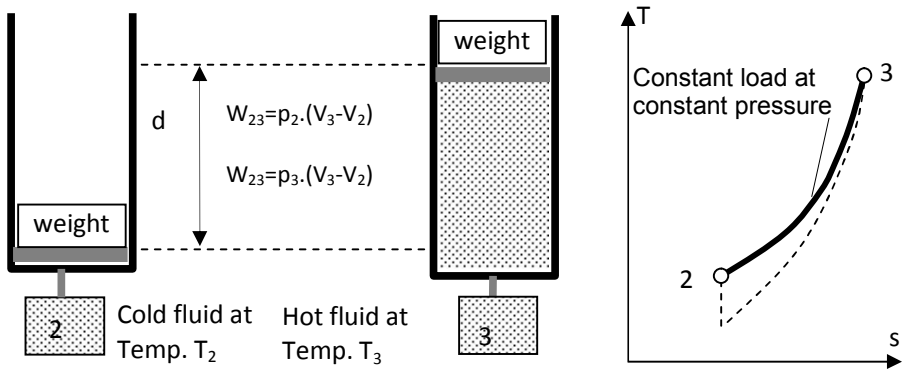

Fig. 2. Process of heating a fluid at constant pressure (closed process), where fluid is confined in a heater and a cylinder as heat is added

The conversion ratio $C_R = \eta_{23}$ of this closed reversible transformation (2)–(3) is

$$C_R = \eta_{23} = \frac{W_{23}}{q_{23}} = \frac{q_{23} - \Delta u_{23}}{q_{23}} = 1 - \frac{\Delta u_{23}}{q_{23}} = 1 - \frac{Cv \cdot (T_3 - T_2)}{Cp \cdot (T_3 - T_2)} = 1 - \frac{1}{\gamma} \tag{3}$$

From Equation (3) it follows that the conversion ratio depends only on the adiabatic expansion coefficient.

2.1.2 The open processes based transformations

Assuming now that heat is added to a unit mass of WF following an isobaric path function along the transformation (2)–(3), as shown in Fig. 3, where the WF is circulating so that the process (2–3) is assumed to be an open transformation, the process (2)–(3) of heat absorption is associated with the expansion of the gas, causing the specific volume to increase from v_2 to v_3, the temperature from T_2 to T_3, the enthalpy from h_2 to h_3, and the entropy from s_2 to s_3.

The first principle for an open system where internal irreversibilities and potential and kinetic energy are neglected yields

$$q_{23} - W_{23} = \Delta h_{23} \tag{4}$$

Therefore, the finite quantity of heat q_{23} added to the system is described as

$$q_{23} = \Delta h_{23} + W_{23} = (h_3 - h_2) + p_2 \cdot (V_3 - V_2) \tag{5}$$

The conversion ratio of this open transformation (2)–(3) is

$$C_R = \eta_{23} = \frac{W_{23}}{q_{23}} = \frac{q_{23} - \Delta h_{23}}{q_{23}} = 1 - \frac{\Delta h_{23}}{q_{23}} = \frac{W_{23}}{\Delta h_{23} + W_{23}} = \frac{R}{Cp + R} = \frac{\gamma - 1}{2 \cdot \gamma - 1} \tag{6}$$

The conversion ratio achieved in (6) for the open system is lower than the conversion ratio achieved in (3) for the closed system. This is because the change in internal energy Δu_{23} in (4) is less than the change of enthalpy Δh_{23} in (6). Thus, with regard to helium, nitrogen, and hydrogen, the corresponding conversion ratios are approached from (6) as $C_{R\_He} \approx 0.285$ for helium, $C_{R\_N2} \approx 0.22$ for nitrogen, and $C_{R\_H2} \approx 0.22$ for hydrogen. It must be noted that these values have been computed for an open transformation which occurred under a wide range of pressures and temperatures which were practically constant (in the case of nitrogen, the observed change was from 0.224 to 0.216 when the pressure changed from 10 to 100 bar and the temperature changed from 400 to 800 K), which means that the ratio of conversion of heat into mechanical work under an open transformation does not depend significantly on the pressure or temperature at which such a transformation is carried out. The conversion ratios of closed- and open-system-based transformations for helium,

nitrogen, and hydrogen are summarised in Table 1.

2.2 Analysis of the OPTC

On the basis of the above discussion with regard to the conversion ratios for open processes, the OPTC (a non-regenerative trilateral cycle) consisting of open processes, as shown in Fig. 4, is analysed. The structure of the engine characterised by an isobaric expansion-based OPTC (at constant load) coupled to a thermal to hydraulic energy convertor is depicted in Fig. 4, where Fig. 4 (a) shows the OPTC's physical structure with two single-acting cylinders, Fig. 4 (b) the OPTC's physical structure with a double-acting cylinder, Fig. 4 (c) the T-s diagram, and Fig. 4 (c) the p-v diagram.

Table 1. The conversion ratio

	Eq. (3)	Eq. (6)
C_R model	$C_R = 1 - \frac{1}{\gamma}$	$C_R = \frac{\gamma - 1}{2 \cdot \gamma - 1}$
He	0.4	0.285
N_2	0.33	0.22
H_2	0.29	0.22

The OPTC consists of a closed cycle operating with hydrogen, helium, or nitrogen as WF in which the transformations associated with the cycle undergo some exchange of matter so that the cycle transformations are open systems. The energy balance corresponding to the OPTC assuming open processes, since there is exchange of matter, is performed according to the T-s and p-v diagrams of Figs. 4(c) and (d), as follows:

$$q_{23} - q_{31} - W_{23} + W_{12} = 0 \tag{7}$$

The amount of specific energy added from an external heat source is defined as

$$\begin{aligned} q_i &= \Delta h_{23} + W_{23} = (h_3 - h_2) + W_{23} \\ &= (h_3 - h_2) + p_2(V_3 - V_2) \end{aligned} \tag{8}$$

The amount of heat rejected to the low temperature heat sink is

$$q_o = \Delta h_{31} = (h_3 - h_1) \tag{9}$$

Hence, the net work is defined as

$$W_N = q_i - q_o = W_{23} - W_{12} = W_{23} + h_1 - h_2 \tag{10}$$

and the thermal efficiency is given as

$$\eta_{NR} = \frac{W_N}{q_i} = \frac{q_i - q_o}{q_i} = \frac{W_{23} + h_1 - h_2}{W_{23} + h_3 - h_2} \tag{11}$$

2.3. Analysis of the ROPTC

The structure of the ROPTC is shown in Fig. 5 as well as its corresponding T-s diagram. The thermal efficiency of the ROPTC is computed assuming an isobaric expansion process along the transformation (2–3), which undergoes open process behaviour.

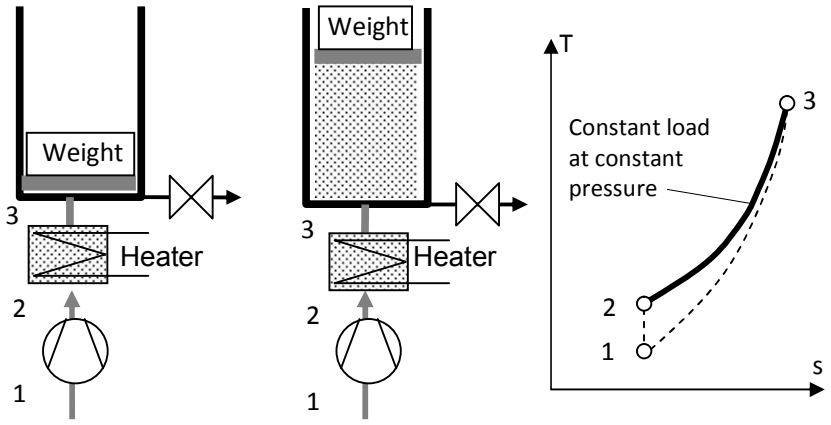

Fig. 3. Process of heating a fluid at constant pressure, where the fluid is transferred from a reservoir to a heater as heat is added (open system)

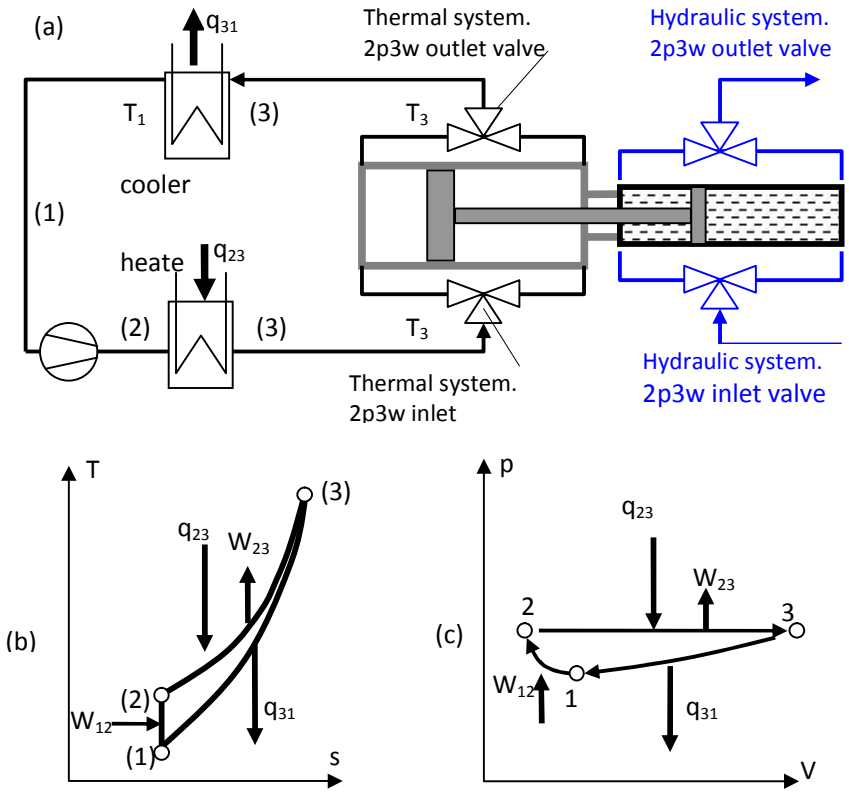

Fig. 4. OPTC-based engine principle: (a) the OPTC's physical structure with a double-acting cylinder; (b) T-s diagram; (c) p-v diagram

As shown in Fig. 5, the plant structure is composed of two independent circuits (thermal and hydraulic). In the proposed ROPTC-based engine, assuming that the corresponding inlet and outlet two-position three-way valves are in the correct position, the heated fluid at point (3) of the T-s diagram of Fig. (a), at high pressure p_3 and temperature T_3, flows into the thermal cylinder, which pushes down the corresponding piston and transfers mechanical work to the hydraulic cylinder. Consequently, the evacuated heat transfer fluid at high temperature T_3 is cooled first in the regenerator, reaching the temperature T_{3x}, and further in the cooler to approach the temperature T_1. The compressor takes the cooled gas from the cooler and transfers it at temperature T_2 to the regenerator, where it reaches temperature T_{2x}. From the regenerator at temperature T_{2x}, it passes through the heater, acquiring the temperature T_3, so that the thermal cycle is completed. The following semi-cycle is performed by interchanging the role of each side of the cylinder. Summarising, the role of each side of the gas cylinder is reversed every semi-cycle.

In the considered analysis, as shown in Fig. 5, the WF (helium, nitrogen, or hydrogen) at low pressure conditions, state point (1) with temperature and pressure (p_1, T_1) at the compressor suction side, is compressed and acquires the pressure and temperature of the state point (2) (p_2, T_2), as shown in the T-s diagram depicted in Fig. 5(b).

As fluid is added to the heater, an amount of heat q_{23} at constant pressure is also added to the fluid, contributing to the increase of the specific volume, temperature, enthalpy, and entropy (V_3, T_3, h_3, s_3). Simultaneously, the heated fluid expands at constant pressure into the cylinder, causing the conversion of part of the added heat energy into mechanical work, while the rest of the added heat remains in the cylinder as residual heat. After this isobaric process ends, the fluid contained in the cylinder at temperature T_3 is exhausted toward the compressor suction side through a heat exchanger or regenerator to recover part of the heat rejected during the process (3)–(3x). The amount of residual heat remaining in the cylinder between points (3x) and (1) that cannot be recovered must be rejected to

the environment by means of a cooler, reaching state (1).

The compressor work along the transformation (1)–(2) is defined as

$$W_{12} = (h_2 - h_1) \tag{12}$$

The amount of specific energy added to the transformation (2)–(3) is defined as

$$q_{23} = \Delta h_{23} + W_{23} = (h_3 - h_2) + p_2(V_3 - V_2) \tag{13}$$

The amount of heat that can be regenerated is defined as

$$q_R = (h_3 - h_{3x}) \tag{14}$$

where the maximum regenerative capacity is achieved when $(T_3 - T_{3x}) = (T_3 - T_2)/2$.

The net heat q_i supplied from a heat source to the cycle is

$$q_i = q_{23} - q_R = \Delta h_{23} + W_{23} - (h_3 - h_{3x}) = W_{23} - h_2 + h_{3x} \tag{15}$$

The amount of heat rejected to the low temperature heat sink is

$$q_o = (h_{3x} - h_1) \tag{16}$$

Hence the net work W_N is defined as

$$W_N = q_i - q_o = W_{23} - W_{12} = W_{23} - h_2 + h_1 \tag{17}$$

and the thermal efficiency is given as

$$\eta_R = \frac{W_N}{q_i} = \frac{q_i - q_o}{q_i} = \frac{W_{23} - h_2 + h_1}{W_{23} - h_2 + h_{3x}} \tag{18}$$

Since the beneficial effect of the regeneration is simply to avoid as much as possible the rejection of useful heat to the heat sink, this suggests that the ROPTC provides higher thermal efficiency into the range of low temperatures compared with the Carnot factor.

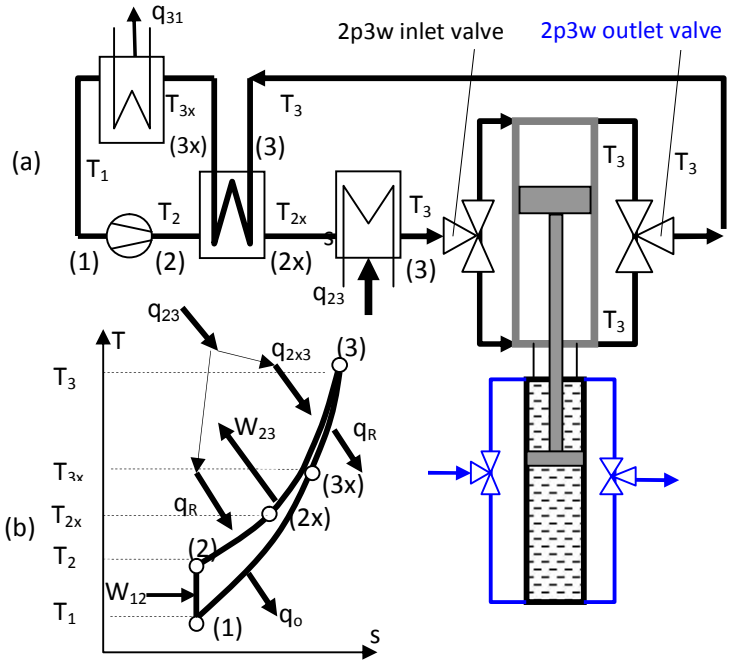

Fig. 5. Structure of the ROPTC: (a) the basic plant structure; (b) the corresponding T-s diagram

3. A CASE STUDY APPLIED TO THE OPTC AND THE ROPTC

Fig. 5 depicts two options for the plant structure. The plant structure shown in Fig. 5(a) is composed of two independent circuits (thermal and hydraulic). The thermal power conversion system is implemented by at least one tandem actuating cylinder. Both thermal and hydraulic circuits are coupled by means of the tandem cylinders in such a way that the thermal cylinder drives the hydraulic cylinder. A tandem actuating cylinder consists of two double-acting cylinders arranged one behind the other but designed as a single unit. This type of actuating cylinder is used in applications that require two or more independent systems. The flow of fluid to and from the two chambers of the tandem actuating cylinder is provided by two independent circuits: the ROPTC system and the hydraulic system. The role of each side of the gas and hydraulic cylinder is reversed every semi-cycle. The hydraulic transfer fluid flows through the hydraulic motor, which drives the generator to allow conversion into electrical energy.

In order to determine the performance of the OPTC and the ROPTC, the thermal analysis of the case study is carried out under the following conditions: The compressor isentropic efficiency is 0.85; the maximum regeneration capacity is assumed for $T_{2x} = T_{3x}$, which requires a regenerator effectiveness given as the ratio of the temperature difference ($T_{2x} - T_2$) to the temperature difference ($T_3 - T_2$) of 0.50; and the WF data properties are taken from the database REFPROP, referenced in [3] for real gases represented in Tables A1 to A3 of Appendix A. Computations performed on the data of Tables A1 to A3 of Appendix A refer to the T-s diagram in Figs. 4(b) and 5(b).

3.1 Analysis of Results and Discussion

A study of the OPTC was performed under the assumption that the structure of the ROPTC is similar to that of the OPTC with the regenerator out of use. The analysis carried out with regard to the heat energy conversion ratio, for which the results are shown in Table 1, highlights relevant features as follows:

- The conversion ratio for an open thermodynamic transformation is significantly lower than that for a closed transformation, and
- The value of the conversion ratio for each fluid remains practically constant even though temperature and pressure change significantly.

With respect to the OPTC, for each analysed WF (hydrogen, helium, and nitrogen) within the range of top temperatures between 310 and 400 K, the data of interest corresponding to the state points of the T-s diagram shown in Fig. 4 (b) are represented in Table A4, showing the thermal efficiency, Carnot factor, and specific work as functions of the top temperature T_3. Fig. 6 depicts the thermal efficiency and CF of the OPTC.

With respect to the ROPTC, for each analysed WF (hydrogen, helium, and nitrogen) within the range of top temperatures between 310 and 550 K, the data of interest corresponding to the state points of the T-s diagram shown in Fig. 5 (b) are represented in Table A4, showing the thermal efficiency, Carnot factor, and specific work as functions of the top temperature T_3. Fig. 7 depicts the thermal efficiency and CF of the ROPTC. Under the assumed operating conditions given in Table A4, Fig. 7 highlights the differences in thermal efficiency with respect to the Carnot factor for a range of temperatures between 320 and 550 K. It is observed that as temperature T_3 surpasses certain values, the Carnot factor will surpass the values of the thermal efficiencies.

In Figs. 6 and 7, the behaviour of helium as WF in terms of thermal efficiency shows that whereas nitrogen renders low efficiency and low specific work according to the data of Table A4, and hydrogen renders low efficiency but high specific work, helium satisfies both requirements: Good thermal efficiency and acceptable specific work at low temperatures. For medium and high temperatures, however, the OPTC is discarded because of its poorer thermal efficiency.

The achieved curves indicate that in terms of thermal efficiency the diatomic hydrogen and nitrogen profiles are very similar. Nevertheless, helium is slightly superior. In terms of specific work, as shown in Fig. 8, it happens that hydrogen develops much more specific work than nitrogen. The inherent characteristics of the hydrogen in terms of handling and safety precautions suggest, however, that the safest available fluid, such as helium, should be chosen. Helium offers acceptable efficiency and specific work, broadly satisfying both requirements. The effect of low specific work, as

in the case of nitrogen as WF, contributes to the increasing volume of the plant for the same demanded power.

Several operating parameters have a significant negative effect on the ROPTC's thermal efficiency. Thus, besides the general known irreversibilities, the effect of the temperature difference [$T_3 - T_{3x}$] in the regenerator is remarkable. The influence of the temperature difference [$T_3 - T_{3x}$] on the thermal efficiency is shown in Table 2, where for a temperature difference ranging from 0 to 35 K the efficiency changes from 24.3 to 41.1% when helium is used as the WF.

Another important factor affecting the thermal efficiencies of the OPTC and ROPTC is the pressure ratio Pr = [p_2/p_1]. Thus, Table 3 shows the thermal efficiencies and specific work for pressure ratios ranging from 1.013 to 1.067 with the data from Table A6 in [20]. As shown in Table 3, for a pressure ratio ranging from Pr = [p_2/p_1] = [400/395] = 1.012 to Pr = [p_2/p_1] = [400/375] = 1.067, the thermal efficiencies decrease from 41.7 to 2.4 for the ROPTC and from 24.3 to 1.7 for the OPTC with helium as WF. In the same way the specific work decreases accordingly from 119.26 to 61.68 kJ/kg.

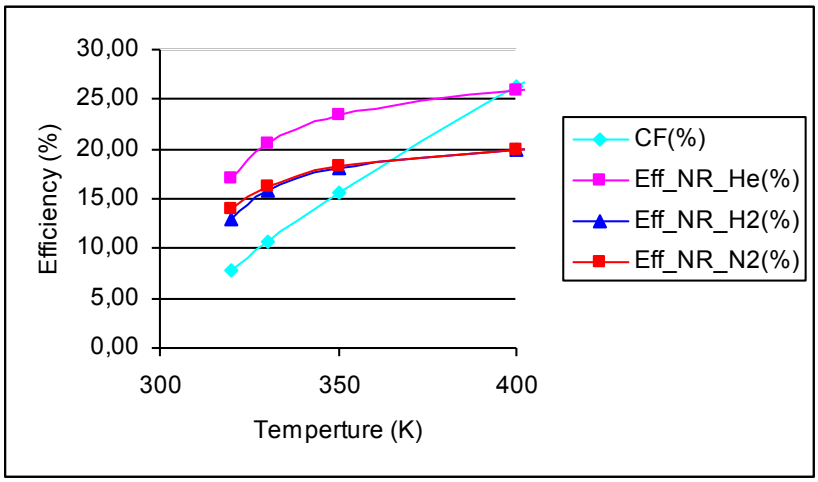

Fig. 6. Thermal efficiency (Eff_NR) of the OPTC and the CF for helium, nitrogen, and hydrogen as WFs

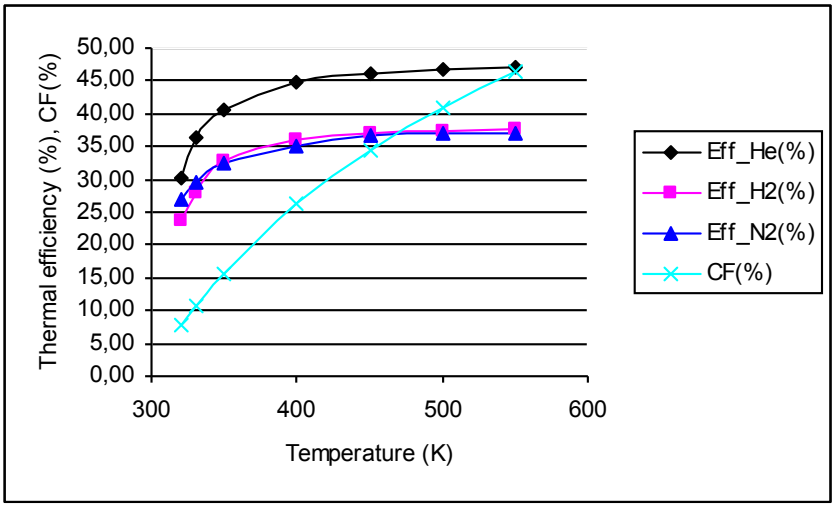

Fig. 7. Thermal efficiency (Eff) of the ROPTC and the CF for helium, nitrogen, and hydrogen as WFs

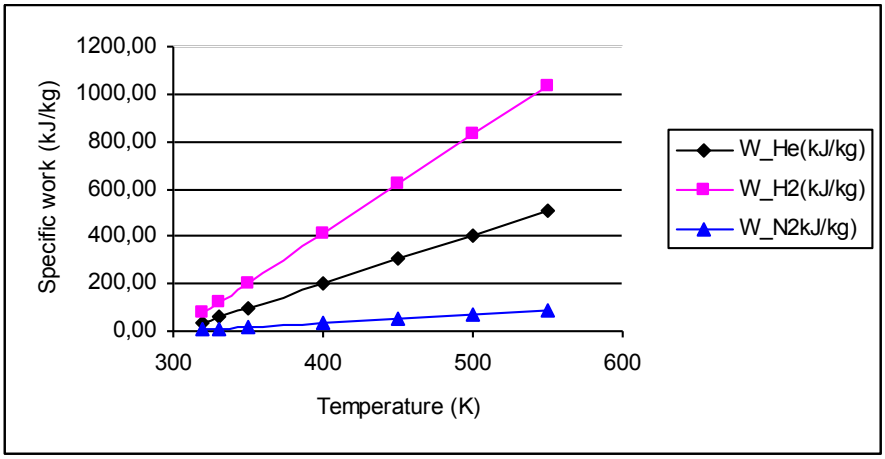

Fig. 8. Specific work corresponding to both the OPTC and the ROPTC for hydrogen, helium, and nitrogen as WFs

Table 2. Results of the analysis of the thermal efficiency of the ROPTC based on the data of Table A5 from [20] as a function of the temperature difference $[T_3 - T_{3x}]$ of the regenerator for T_3 = 360 K and helium as WF

$[T_3 - T_{3x}]$ (K)	0	15	20	25	30	35
η_{NR}(%)	24.29	24.29	24.29	24.29	24.29	24.29
CF(%)	18	18	18	18	18	18
η (%)	24.29	29.53	31.76	34.37	37.44	41.11

Table 3. Results of the analysis of the thermal efficiency and specific work of the OPTC and the ROPTC based on the data from Table A6 in [20] as a function of the pressure ratio $[p_2/p_1]$ for helium at a temperature of T_3 = 360 K

Pr	1.013	1.026	1.039	1.053	1.067
η (%)	41.7	36	26.6	20.4	2.4
η_{NR}(%)	24.3	20.4	14.5	10.9	1.7
CF (%)	18	18	18	18	18
W (kJ/kg)	119.26	106.89	90.94	80.91	61.68

Such a dramatic decrease in efficiency as a function of the pressure ratio suggests that a design with pressure ratios sufficiently low for acceptable efficiency to be achieved should be selected. Nevertheless, decreasing the pressure ratios demands a large plant structure for all involved parts, so that a compromise that relates both concepts must be assumed.

4. CONCLUSION

A regenerative trilateral thermal cycle called ROPTC, which converts heat to mechanical work as heat is absorbed along an isobaric expansion-based process, has been proposed. It differs from the quadrilateral Carnot-based cycles in that the thermal WF absorbs heat from a heat source and simultaneously, in the same cycle's isobaric process, converts a fraction of this heat into mechanical work. The proposed ROPTC is seen to operate with hydrogen, helium, and nitrogen as WFs. According to the characteristics of the new ROPTC, expressions for thermal efficiency have been achieved and analysed.

The performance results of the ROPTC have been compared with the results obtained for the Carnot cycle under the same range and ratio of temperatures. The most important conclusion relates to the theoretical thermal efficiency of the cycle, which exceeds the Carnot factor under appropriate operating conditions.

This controversial result suggests that even though the Carnot factor is a limitation of Carnot-based engines it does not affect the thermal efficiency of thermal cycles based on isobaric expansion processes. Furthermore, even at very low temperatures the Carnot factor can be overcome, as shown in Table A4 for both the OPTC (without regeneration) and the ROPTC. The reason is that in the proposed trilateral cycle, isobaric heat absorption and simultaneous

conversion into mechanical work and residual heat take place simultaneously during a cycle transformation. Furthermore, thermal losses due to isentropic efficiency are significantly reduced since the conventional adiabatic expansion associated with inherent isentropic efficiency is avoided.

The efficiency enhancement with respect to quadrilateral Carnot-based cycles is due to the following:

- The fact that the cycle absorbs thermal energy and simultaneously converts a fraction of heat into both mechanical work and high grade residual heat without the losses inherent in isentropic efficiency;
- Regeneration of the exhausted residual high grade heat;
- The selected WF's inherent characteristics and behaviour;
- The chosen operating parameters (pressure ratio, working pressures and temperatures).

There are, however, some disadvantages which contribute negatively to the thermal efficiency of the cycle; thus, apart from the known inherent irreversibilities, the regenerator capacity and the operating pressure ratio are important parameters to take into account.

As revealed in the results, the thermal efficiency is significantly increased in comparison with the conventional ORCs under realisable conditions. The ability to obtain high thermal efficiencies only at low temperatures will take advantage of the use of industrial waste heat as a power source in the OPTC and ROPTC with acceptable efficiency. Finally, the widespread use of residual heat as a power source also contributes to the reduction of fossil fuel consumption, since the more efficient use of source energy reduces the global warming potential.

COMPETING INTERESTS

Authors have declared that no competing interests exist.

REFERENCES

1. Hung TC, Shai TY, Wang SK. A review of Organic Rankine Cycles (ORCs) for the recovery of low-grade waste heat. Energy. 1999;22(7):661-7.
2. Yamamoto T, Furuhata T, Arai N, Mori K. Design and testing of the Organic Rankine Cycle. Energy. 2001;26(3):239-251.
3. Angelino G, Colonna P. Multicomponent WFs for Organic Rankine Cycles (ORC), Energy. 1998;23(6):449-63.
4. Saleh B, Koglbauer G, Wendland M, Fischer J. WFs for low temperature Organic Rankine Cycles. Energy. 2006;32(7):1210-2021.
5. Borsukiewicz-Gozdur A, Nowak W. Comparative analysis of natural and synthetic refrigerants in application to low temperature Clausius-Rankine cycle. Energy. 2007;32(4):344-52.
6. Mago PJ, Chamra LM, Srinivasan K, Somayaji C. An examination of regenerative Organic Rankine Cycles using dry fluids. Applied Thermal Engineering. 2008;28:998-1007.
7. Wang ZQ, Zhou NJ, Guo J, Wang XY. Fluid selection and parametric optimization of organic Rankine cycle using low temperature waste heat. Energy. 2012;40:107-15.
8. Jianqin F, Jingping, Chengqin R, Linjun W, Banglin D, Zhengxin X. An open steam power cycle used for IC engine exhaust gas energy recovery. Energy. 2012;44:544-54.
9. Dongxiang W, Xiang L, Hao P, Lin L, Lan LT. Efficiency and optimal performance evaluation of organic Rankine cycle for low grade waste heat power generation. Energy. 2013;50:343-52.
10. Najjar YSH. Efficient use of energy by utilizing gas turbine combined systems. Applied Thermal Engineering. 2001;21:407-38.
11. Chacartegui R, Sánchez D, Muñoz JM, Sánchez T. Alternative ORC bottoming cycles for combined cycle power plants. Applied Energy. 2009;86:2162-70.
12. Invernizzi C, Iora P, Silva P. Bottoming micro-Rankine Cycles for micro-gas turbines. Applied Thermal Engineering. 2007;27:100-110.
13. Tchanche BF, Lambrinos G, Frangoudakis A, Papadakis G. Low-grade heat conversion into power using organic Rankine cycles – A review of various applications. Renewable and Sustainable Energy Reviews. 2011;15:3963-79.
14. Sprouse C, Depcik C. Review of organic Rankine cycles for internal combustion engine exhaust waste heat recovery, Applied Thermal Engineering. 2013;51:711-22.

15. Wagar WR, Zamfirescu C, Dincer I. Thermodynamic performance assessment of an ammonia–water Rankine cycle for power and heat production. Energy Conversion and Management. 2010;51:2501-2509.
16. Öhman H, Lundqvist P. Theory and method for analysis of low temperature driven power cycles, Applied Thermal Engineering. 2012;37:44-50. DOI:10.1016/j.applthermaleng.2011.12.046.
17. Ferreiro Garcia R, Ferreiro Sanz B, Ferreiro Sanz C. Contributions on Closed System Transformations Based Thermal Cycles. British Journal of Applied Science & Technology. 2014;4(19):2821-2836
18. Ferreiro Garcia R, Ferreiro Sanz B, Ferreiro Sanz C, Preliminary study of an efficient OTEC Using a thermal cycle with closed thermodynamic transformations. British Journal of Applied Science & Technology. 2014;4(26):3840-3855.
19. Xiaohui S, Yonggao Y, Xiaosong Z. Thermodynamic analysis of a novel energy-efficient refrigeration system subcooled by liquid desiccant dehumidification and evaporation. Energy Conversion and Management. 2014;(78):286-296.
20. Lemmon EW, Huber ML, McLinden MO. NIST Reference Fluid Thermodynamic and Transport Properties - REFPROP Version 8.0, User's Guide, NIST 2007, Boulder, Colorado; 2007.

Appendix A

Table A1. Data for the performance analysis as a function of the top temperature T_3 for helium as WF from [20]

Point	T(K)	h(kJ/kg)	u(kJ/kg)	s(kJ/kg-K)	p(bar)	v(m^3/kg)
T_3 = 550						
1	295	1663	936.72	15.561	395	0.018387
2	296.44	1673.71	941.39	15.561	400	0.018267
3	550	2983.5	1734	18.758	400	0.031237
3x	403	2222.2	1275	17.177	395	0.023979
2x	402.00	2218.60	1272.1	17.138	400	0.023663
T_3 = 500						
3	500	2725.1	1578.1	18.266	400	0.028676
3x	382	2113.6	1209.4	16.9	395	0.022891
2x	381.25	2111.30	1207.2	16.864	400	0.022602
T_3 = 450						
3	450	2466.7	1422	17.721	400	0.026118
3x	361	2004.9	1143.7	16.607	395	0.021804
2x	360.50	2003.90	1142.3	16.575	400	0.021541
T_3 = 400						
3	400	2208.2	1265.8	17.112	400	0.023561
3x	340	1896.2	1077.9	16.297	395	0.020717
2x	339.74	1896.40	1077.2	16.268	400	0.020480
T_3 = 350						
3	350	1949.6	1109.4	16.422	400	0.021005
3x	320	1792.6	1015.2	15.983	395	0.019682
2x	318.26	1785.20	1009.9	15.929	400	0.019382
T_3 = 330						
3	330	1846	1046.7	16.117	400	0.019982
3x	311	1746	986.97	15.835	395	0.019216
2x	310.37	1744.30	985.13	15.799	400	0.018979
T_3 = 320						
3	320	1794.2	1015.3	15.957	400	0.019471
3x	307	1725.3	974.41	15.768	395	0.019009
2x	306.06	1721.90	971.6	15.727	400	0.018758

Table A2. Data for the performance analysis as a function of the top temperature T_3 for hydrogen as WF from [20]

Point	T(K)	h(kJ/kg)	u(kJ/kg)	s(kJ/kg-K)	p(bar)	v(m^3/kg)
T_3 = 550						
1	295	4112.8	2588.6	28.3800	395	0.038587
2	296.44	4135.51	2599.4	28.3800	400	0.038319
3	550	7890.4	5298	37.5540	400	0.064810
3x	408	5792.7	3793.3	33.2010	395	0.050618
2x	406.92	5780.40	3781.5	33.1100	400	0.049973
T_3 = 500						
3	500	7154.9	4769.2	36.1520	400	0.059642
3x	386	5466.6	3559.1	32.3800	395	0.048291
2x	385.19	5458.30	3550.1	32.2960	400	0.047703
T_3 = 450						
3	450	6417.6	4239.3	34.5980	400	0.054498
3x	364	5139.9	3324.5	31.5090	395	0.045958
2x	363.42	5135.00	3318	31.4320	400	0.045423
T_3 = 400						
3	400	5677.9	3707.9	32.8560	400	0.049251

Point	T(K)	h(kJ/kg)	u(kJ/kg)	s(kJ/kg-K)	p(bar)	v(m^3/kg)
3x	342	4812.8	3089.9	30.5820	395	0.043724
2x	341.69	4811.80	3086.2	30.5150	400	0.043140
T_3 = 350						
3	350	4935.4	3174.9	30.8730	400	0.044014
3x	320	4485.3	2855.2	29.5920	395	0.041268
2x	319.90	4487.30	2853.6	29.5340	400	0.040843
T_3 = 330						
3	330	4637.7	2961.4	29.9970	400	0.041909
3x	312	4366.1	2769.8	29.2410	395	0.040411
2x	310.55	4348.00	2753.8	29.0920	400	0.019522
T_3 = 320						
3	320	4488.8	2854.7	29.5380	400	0.040853
3x	307	4291.6	2716.5	28.9740	395	0.039785
2x	306.66	4289.90	2712.2	28.9030	400	0.039441

Table A3. Data for the performance analysis as a function of the top temperature T_3 for nitrogen as WF from [20]

Point	T(K)	h(kJ/kg)	u(kJ/kg)	s(kJ/kg-K)	p(bar)	v(m^3/kg)
T_3 = 550						
1	295	264.41	155.57	4.8849	395	0.002756
2	296	266.02	156.07	4.8849	400	0.002743
3	550	579.55	381.86	5.6568	400	0.004942
3x	406	407.94	259.3	5.2992	395	0.003763
2x	404.56	406.26	257.64	5.2904	400	0.003716
T_3 = 500						
3	500	520.94	339.79	5.5451	400	0.004529
3x	384	380.68	239.74	5.2301	395	0.003568
2x	383.67	380.34	239.04	5.2246	400	0.003533
T_3 = 450						
3	450	461.48	297.2	5.4198	400	0.004107
3x	362	352.95	219.8	5.1558	395	0.003371
2x	362.85	354.08	220.16	5.1543	400	0.003348
T_3 = 400						
3	400	400.64	253.61	5.2764	400	0.003676
3x	342	327.23	201.26	5.0827	395	0.003189
2x	340.40	325.19	199.31	5.072	400	0.003147
T_3 = 350						
3	350	337.63	208.29	5.1081	400	0.003233
3x	320	298.3	180.3	4.9952	395	0.002987
2x	319.28	297.36	179.13	4.9876	400	0.002956
T_3 = 330						
3	330	311.57	189.45	5.0314	400	0.003053
3x	311	286.23	171.52	4.957	395	0.002904
2x	310.86	286.06	170.9	4.9518	400	0.002879
T_3 = 320						
3	320	298.32	179.83	4.9906	400	0.002962
3x	307	279.47	166.58	4.935	395	0.002858
2x	307.01	280.84	167.09	4.9349	400	0.002844

Table A4. The thermal efficiency and the specific work of the OPTC and ROPTC compared with those of the CF for maximum cycle temperatures T_3 in the range of 320 and 550 K for hydrogen, helium, and nitrogen as WFs, assuming a bottom temperature T_1 of 295 K

T_3 (K)	550	500	450	400	350	330	320
CF	46.36	41.00	34.44	26.25	15.71	10.61	7.81
Helium							
η_He (%)	47.07	46.71	46.12	44.94	40.47	36.25	30.04
η_{NR} He (%)	27.4	27.1	26.7	25.9	23.5	20.5	17
W_He (kJ/kg)	508.10	405.65	303.33	201.00	98.81	57.89	37.45
Hydrogen							
η_H_2 (%)	37.69	37.36	36.94	35.89	32.87	27.93	23.83
η_{NR}_H_2 (%)	21.2	21	20.7	20	18.15	15.8	13
W_H_2 (kJ/kg)	1037.00	830.20	624.50	414.60	205.10	120.90	78.65
Nitrogen							
η_N_2 (%)	37.13	36.98	36.71	35.19	32.62	29.64	26.97
η_{NR}_N_2 (%)	21.2	21	20.7	20	18.3	16.3	14
W_N_2 (kJ/kg)	86.40	69.80	53.00	35.70	18.00	10.80	7.20

Table A5. Data for the analysis of the thermal efficiency as a function of the temperature difference [$T_3 - T_{3x}$] of the regenerator for T_3 = 360 K and helium as WF

Point	T(K)	h(kJ/kg)	u(kJ/kg)	s(kJ/kg-K)	p(bar)	v(m^3/kg)
1	295	1663	936.72	15.561	395	0.018387
2	296.44	1673.71	941.39	15.561	400	0.018267
3	360	2001.3	1140.7	16.567	400	0.021516
T3 – T3x = 0 K						
3x	360	1999.8	1140.5	16.593	395	0.021753
2x	296.65	1673.10	942.04	15.565	400	0.018277
T3 – T3x = 15 K						
3x	345	1922.1	1093.6	16.373	395	0.020976
2x	307.44	1729.10	975.93	15.75	400	0.018829
T3 – T3x = 20 K						
3x	340	1896.2	1077.9	16.297	395	0.020717
2x	311.04	1747.80	987.1	15.81	400	0.019013
T3 – T3x = 25 K						
3x	335	1870.3	1062.2	16.221	395	0.020458
2x	314.64	1766.40	998.53	15.87	400	0.019197
T3 – T3x = 30 K						
3x	330	1844.4	1046.6	16.143	395	0.020199
2x	318.24	1785.10	1009.8	16.929	400	0.019381
T3 – T3x = 35 K						
3x	325	1818.5	1030.9	16.064	395	0.019941
2x	321.83	1799.40	1018.5	15.974	400	0.019522

Table A6. Data for the analysis of the thermal efficiency and specific work as a function of the pressure ratio [p_2/p_1] for helium at temperature T_3 = 360 K

Point	T(K)	h(kJ/kg)	u(kJ/kg)	s(kJ/kg-K)	p(bar)	v(m^3/kg)
[p_2/p_1] = 400/395						
1	295	1663	936.72	15.561	395	0.018387
2	296.44	1673.71	941.39	15.561	400	0.018267
3	360	2001.3	1140.7	16.567	400	0.021516
3x	324	1814.9	1027.9	16.022	395	0.019676
2x	322.33	1806.30	1022.7	15.995	400	0.019590
[p_2/p_1] = 400/390						
1	295	1663	936.59	15.587	390	0.018586

Point	T(K)	h(kJ/kg)	u(kJ/kg)	s(kJ/kg-K)	p(bar)	v(m^3/kg)
2	297.93	1683.03	946.07	15.587	400	0.018343
3	360	2001.3	1140.7	16.567	400	0.021516
3x	325	1817	1030.7	16.09	390	0.020160
2x	323.63	1813.00	1026.6	16.016	400	0.019657
$[p_2/p_1]$ = 400/385						
1	295	1659.9	936.46	15.614	385	0.018791
2	299.5	1692.72	950.95	15.614	400	0.018422
3	360	2001.3	1140.7	16.567	400	0.021516
3x	326	1820.6	1033.7	16.132	385	0.020438
2x	324.79	1819.00	1030.4	16.034	400	0.019716
$[p_2/p_1]$ = 400/380						
1	295	1663	936.32	15.641	380	0.019001
2	301.5	1702.65	955.86	15.641	400	0.018502
3	360	2001.3	1140.7	16.567	400	0.021516
3x	327	1824.2	1036.7	16.174	380	0.020724
2x	326.21	1826.40	1034.8	16.057	400	0.019789
$[p_2/p_1]$ = 400/375						
1	295	1656.8	936.19	15.668	375	0.019216
2	302.62	1712.45	960.8	15.668	400	0.018583
3	360	2001.3	1140.7	16.567	400	0.021516
3x	328	1827.8	1039.7	16.217	375	0.021017
2x	327.13	1831.50	1038	16.073	400	0.019840

Peer-review history:
The peer review history for this paper can be accessed here:
http://www.sciencedomain.org/review-history.php?iid=770&id=5&aid=7694